

COSMIC MICROWAVE BACKGROUND FILTERS AND THE DARK FLOW MEASUREMENT

F. ATRIO-BARANDELA¹, A. KASHLINSKY², H. EBELING³, D. KOCEVSKI⁴

Draft version November 6, 2018

ABSTRACT

Recent measurements of large-scale peculiar velocities from the cumulative kinematic Sunyaev-Zel'dovich effect using WMAP data and X-ray selected clusters from ROSAT have identified a bulk flow of galaxy clusters at $\sim 600 - 1,000 \text{ km s}^{-1}$ on scales of $\sim 0.5 - 1 \text{ Gpc}$, roughly aligned with the all-sky Cosmic Microwave Background (CMB) dipole. The flow is inferred from the detection of a residual dipole generated by CMB fluctuations exclusively in the direction of galaxy clusters, and measured within apertures containing zero monopole. Consistent with this interpretation, the amplitude of the dipole correlates with the X-ray luminosity of the clusters. To enable this measurement, the CMB data need to be filtered to remove the primary CMB, thereby increasing the data's signal-to-noise ratio. Filtering cannot imprint a signal with the mentioned properties at cluster positions; however, an inadequately designed filter can greatly suppress such a signal. We show here that recent studies that failed to detect a large-scale flow with various filters indeed adopted flawed implementations; when correctly implemented, these alternative filters lead to results that are in fact consistent with the Dark Flow signal. The discrepancies can be traced to the likely presence of residual dipoles caused by the thermal Sunyaev-Zel'dovich effect, to assumptions about cluster profiles incompatible with the data as well as failure to compute dipoles at the zero monopole aperture. PLANCK maps, with their large frequency coverage and a 217 GHz channel, will be instrumental to probe bulk flows, to remove spurious dipole signals and to help identify filtering schemes appropriate for this measurement.

Subject headings: cosmology: cosmic microwave background, cosmology: large-scale structure of the universe, cosmology: observations

1. INTRODUCTION.

Peculiar velocities are deviations from the uniform expansion of the Universe. In the standard gravitational-instability paradigm, they are generated by inhomogeneities in the matter distribution. Measurements of peculiar velocities using galaxies rely on distance indicators to subtract the Hubble expansion, which limits the volume probed to $\sim 100h^{-1} \text{ Mpc}$ (see Strauss & Willick 1995; Kashlinsky, Atrio-Barandela & Ebeling 2012 for reviews). As an alternative, Kashlinsky & Atrio-Barandela (2000, hereafter KAB) proposed a method to probe the large-scale velocity field via the dipole induced by anisotropies in the CMB temperature that are caused by the kinematic Sunyaev-Zel'dovich (SZ; Sunyaev & Zel'dovich 1970, 1972) effect in the direction of clusters of galaxies. The SZ has two components: a thermal one (TSZ), caused by the thermal motions of electrons in the potential wells of clusters, and a kinematic one (KSZ), caused by the motion of the cluster as a whole (kinematic SZ, KSZ; see e.g. the review by Birkinshaw 1999). Once it is imprinted on the CMB, the SZ distortion remains fixed. It does not depend on distance, making it a very useful tool to detect clusters at high redshift (Planck Collaboration, Planck Early results XXVI, 2011).

The KSZ effect measures motion directly with respect to the CMB frame and does not require subtraction of the Hubble expansion. The KAB method evaluates the dipole from an all-sky CMB temperature map at the locations of known X-ray luminous clusters. Since the main contaminant in foreground clean maps is the primary CMB signal, the data need to be filtered to allow the peculiar velocities of clusters to be measured (Haehnelt & Tegmark 1996); KAB proposed to use a Wiener-type filter for this purpose. In Kashlinsky et al (2008, hereafter KABKE, 2009) we showed that, within cluster apertures containing zero CMB monopole, a residual CMB dipole exists which is aligned with the CMB dipole. The amplitude of this residual dipole scales with cluster X-ray luminosity (Kashlinsky et al 2010; Kashlinsky, Atrio-Barandela & Ebeling 2011) proving that the signal is indeed associated with clusters. We have interpreted this dipole as the signature of a bulk flow. If the flow extends to the cosmological horizon, part of the all-sky CMB dipole could be viewed as being of primordial, rather than kinematic, origin. As of this writing, no alternative interpretations of the signal, which would have been of considerable interest, have been offered in peer-reviewed literature.

Our results have been challenged by other authors. Keisler (2009), as well as the contemporaneous study by Kashlinsky et al (2010), noted that the residuals for each of the maps for the eight WMAP DAs (Differential Assemblies) in the KABKE measurement are correlated, which increases the errors quoted by KABKE, but by no more than $\sqrt{N_{\text{DA}}} = 2.8$, where $N_{\text{DA}} = 8$ is the number of DAs of the WMAP dataset. Keisler then claimed that the detection of a large-scale flow was in fact not statistically significant, his error corrections exceeding the $\sqrt{N_{\text{DA}}}$ factor. Atrio-Barandela et al (2010) pointed out that Keisler (2009) had failed to subtract the dipole of the filtered maps outside

¹ Física Teórica, Universidad de Salamanca, 37008 Salamanca, Spain; atrio@usal.es

² SSAI and Observational Cosmology Laboratory, Code 665, Goddard Space Flight Center, Greenbelt MD 20771; Alexander.Kashlinsky@nasa.gov

³ Institute for Astronomy, University of Hawaii, 2680 Woodlawn Drive, Honolulu, HI 96822; ebeling@ifa.hawaii.edu

⁴ Department of Physics, University of California at Davis, 1 Shields Avenue, Davis, CA 95616, USA; kocevski@physics.ucdavis.edu

the Galactic mask, thereby overestimating his error bars. In addition, we also proved that the filter devised by KAB removes the primary CMB down to the fundamental limit of cosmic variance (Atrio-Barandela et al 2010). It was this highly efficient filtering scheme that allowed a detection of the flow at $3.5\text{--}4\sigma$ confidence level, depending on the cluster sample used. All data needed to verify the measurement have been made publicly available⁵ for examination by the interested reader.

Osborne et al (2011, OMCP) studied the effect of different filters on bulk-flow measurements from WMAP data. In their Appendix B.2 OMCP reproduced our results at the 2.9σ confidence level but failed to notice that this in itself invalidates the statistical uncertainties claimed by Keisler (2009). The lowered significance (compared to our $3.5\text{--}4\sigma$), is due to differences in the catalogs used (Kashlinsky et al 2011) and to the relatively small number of simulations (~ 100) carried out by OMCP to compute the errors. OMCP also implemented alternative, “matched” filters, with which they found no evidence of bulk flows in WMAP data. Those matched filters, however, were designed more to detect radio point sources than to remove the primary CMB anisotropies. As a result, they were insensitive to bulk motions to the extent that the KSZ signal is weaker in the filtered maps than in the original data. As can be seen in OMCP’s Fig. 13, a sample of ~ 730 clusters moving at velocities of $\sim 4,000\text{--}10,000\text{ km s}^{-1}$ is required to produce a detectable signal in the filtered maps. At such extreme velocities, the motion of individual clusters should be detectable directly in the original CMB maps without any need for filtering.

In another study, Mody & Hajian (2012, MH), using a different Wiener filter, concluded that the measured bulk-flow amplitude was “consistent with the Λ CDM prediction”. This statement (made prominently in the MH abstract) is largely meaningless though, since the MH error bars of $1,400\text{--}2,600\text{ km s}^{-1}$ per velocity component render their methodology unable to discriminate between the concordance Λ CDM prediction and a bulk flow of amplitude $600\text{--}1,000\text{ km s}^{-1}$, as measured by KABKE.

In spite of the aforementioned problems with these studies, both the OMCP and MH results have been cited repeatedly as evidence against the existence of a Dark Flow (DF). In this paper, we examine in more detail why the filters used by OMCP and MH failed to detect a statistically significant dipole signal. We stress that our focus is on the dipole signal, *irrespective of its interpretation*. Specifically, we aim to answer the question of why the dipole signal was not detected with the other filtering schemes. Do they reduce the S/N to levels that render the dipole statistically insignificant? Do they redistribute the dipole signal to lie outside the aperture ranges probed there? Equally important, none of the proposed new filters have been demonstrated to probe the same flow than the KAB filter, so the discrepancies between filters could be due to variations of the flow. In this article we will show that the OMCP and MH filters are not as efficient as KAB, but that, when correctly implemented, either filter recovers a signal that is in fact compatible with the DF identified by us. In Sec. 2 we discuss the properties of filters, their effect on the data, and summarize previous results. In Sec. 3 we compute the CMB dipole at the locations of clusters in maps processed with the different filters and discuss their relative merits and their consistency, in Sec. 4 we summarize our results and present our conclusions.

2. KAB METHOD AND CMB FILTERING.

At the positions of clusters, the microwave temperature anisotropies have four main components: the primary CMB, the TSZ and KSZ signal, and instrument noise. In foreground clean maps one needs to expect some level of foreground residuals, but these residuals will not correlate with clusters in the sky and outside the Galactic plane are negligible compared with the cosmological signal. The KSZ anisotropy is given by $\Delta T_{\text{KSZ}} = -T_0\tau(V_{\text{Bulk}}/c)$, where τ is the projected electron density along the line of sight, V_{Bulk} the bulk-flow velocity of our cluster sample, c the speed of light, and T_0 the CMB blackbody temperature. The bulk flow motion of all clusters in a given sample will generate a CMB dipole at the cluster location that we estimated it to be (KAB)

$$a_{1m} = 1\mu\text{K} \left(\frac{V_{\text{bulk}}}{300\text{ km s}^{-1}} \right) \pm 3\mu\text{K} \left(\frac{N_{\text{cl}}}{1,000} \right)^{1/2} \pm 0.6\mu\text{K} \left(\frac{N_{\text{pix}}}{10,000} \right)^{1/2} \pm 0.2\mu\text{K} \left(\frac{N_{\text{cl}}}{1,000} \right)^{1/2} \quad (1)$$

where the terms on the right-hand side describe the contributions from the KSZ, the cosmological CMB, noise, and the TSZ, respectively. In this expression, N_{cl} clusters that occupy a solid angle of N_{pix} pixels in the sky. Instrument noise (the third term) can be further reduced as $N_{\text{DA}}^{-1/2}$ by combining N_{DA} differential assemblies operating at different frequency bands. In addition, the fourth term, reflecting the contribution from the TSZ effect, can be isolated and eliminated by using its distinctive frequency dependence. Nevertheless, the TSZ dipole due to the inhomogeneous distribution of clusters in the sky is bounded above by the TSZ monopole. In Kashlinsky et al (2008, 2009) we proposed to measure dipoles at zero monopole aperture to limit the TSZ dipole contribution even without frequency information.

The largest source of errors in eq. (1) is the sample-variance uncertainty caused by the small number of pixels at which the dipole is evaluated. To determine peculiar velocities it is vital to increase the signal-to-noise ratio (S/N) for these pixels by reducing the contribution from the primary CMB anisotropy. However, unlike for the TSZ component, frequency information can not be used to discriminate between the CMB and KSZ contributions to the overall dipole. To address this problem, KAB proposed to use the statistical properties of the primary CMB to design a filter that effectively removes its contribution while preserving the KSZ component, thereby increasing the S/N of the proposed measurement.

⁵ http://www.kashlinsky.info/bulkflows/data_public

Reflecting the spatial isotropy of the CMB temperature anisotropies, filters are spherically symmetric; in ℓ -space, the filter depends on ℓ but not on m . If $\Delta T = \sum_{\ell m} a_{\ell m} Y_{\ell m}$ and $F(\theta) = (1/4\pi) \sum_{\ell} (2\ell + 1) F_{\ell}^2 P_{\ell}(\cos \theta)$ are the expansions of the temperature map in spherical harmonics and of the filter in Legendre polynomials, respectively, then the filtered map is given by

$$F \star \Delta T = \sum_{\ell m} F_{\ell} a_{\ell m} Y_{\ell m}, \quad (2)$$

where \star denotes convolution. In the following sections we will discuss the distribution of a KSZ dipole in ℓ -space, followed by a brief description of the filters under investigation here.

2.1. The KSZ signal.

Our bulk-flow studies were based on an all-sky cluster sample created by combining the ROSAT-ESO Flux Limited X-ray catalog (REFLEX) (Böhringer et al. 2004) in the southern hemisphere, the extended Brightest Cluster Sample (eBCS) (Ebeling et al. 1998, 2000) in the north, and the Clusters in the Zone of Avoidance (CIZA) (Ebeling et al. 2002; Kocevski et al. 2007) sample along the Galactic plane. Our full catalog contains ~ 1500 entries including clusters and galaxy groups. To illustrate the performance of the different filters, we select a subset of 506 clusters located outside WMAP's KQ75 galactic and point source mask. These clusters are located at redshifts $z \leq 0.16$ and have X-ray luminosities $L_X[0.1 - 2.4 \text{ keV}] \geq 0.5 \times 10^{44} \text{ erg s}^{-1}$. For the purposes of this paper we restrict our analysis to clusters for which the parameters of a β profile (Cavaliere & Fusco-Femiano 1976) have been measured by fitting to ROSAT X-ray data. This sample is smaller than the one used in Kashlinsky et al (2010) and our final statistical significance will be degraded with respect to our earlier results. We divided our set into three independent samples, selected according to luminosity. We define three intervals: $L_X \in ([0.5, 1], [1., 2], [> 2]) \times 10^{44} \text{ erg s}^{-1}$. The distribution of our clusters on the sky is shown in Fig. 1 using a Healpix projection of $N_{\text{side}} = 512$ (Gorski et al., 2005). All clusters are drawn as discs of radius 1.5° .

The set of clusters in the final sample occupies less than 1% of the sky. In such a small solid angle, spherical harmonics are not orthogonal. Before discussing how filters operate, we need to discuss how the dipole power at $\ell = 1$, that is evaluated only at the cluster positions, is redistributed among all multipoles. If $a_{\ell, m}^{\text{KSZ}}$ are the spherical harmonic transforms of the KSZ component of the KSZ dipole evaluated at N_{cl} locations in the sky then the power at each multipole ℓ is $(2\ell + 1)C_{\ell}^{\text{KSZ}} = \sum_m |a_{\ell, m}^{\text{KSZ}}|^2$. We define $S(\ell)$ as the contribution of all multipoles $i \leq \ell$ to the total dipole in the map as:

$$S^2(\ell) = \frac{1}{4\pi} \sum_{i=2}^{\ell} (2i + 1) C_i^{\text{KSZ}}. \quad (3)$$

To predict C_{ℓ}^{KSZ} and $S(\ell)$ we need the electron-density profile of all clusters. Suitable data to derive these profiles accurately are not yet available. To compute the dipole power we will assume that all clusters subtend the same solid angle and move coherently in the direction $(l, b) = (270^{\circ}, 30^{\circ})$. For simplicity we assign a dipole anisotropy $D = -1\mu\text{K}\cos\theta$ to all pixels of each cluster, where θ is the angle between the line of sight of the cluster and the apex of the motion. Figs. 2a and 2b depict the resulting power and the integrated dipole signal $S(\ell)$, respectively, for identical clusters of angular radius $10'$, $15'$ and $30'$. Fig. 2a shows that the lowest multipoles have the largest amplitude, and that power is transferred preferentially to odd multipoles. Fig. 2b shows that less than 10% of the signal remains at $\ell = 1$; the bulk of the signal is contained in the range $1 < \ell < 300$ even for unresolved clusters.

The exact distribution of the KSZ dipole in ℓ -space will depend on the (unknown) profile of clusters and their extent. Since clusters have a radius of $10'$ - $30'$, the effect of the cluster profile will be important for multipoles $\ell > 200 - 600$. Therefore, our conclusion that more than 50% of the KSZ dipole signal lies below those scales is not affected by taking a constant profile. The actual signal will be a combination of the contributions from resolved ($15'$ - $30'$) and unresolved ($10'$) clusters, with clusters of different mass contributing at different relative weights.

2.2. The KAB filter.

The KAB filter was specifically designed to remove the primary CMB of the measured cosmological model. The filter is of the Wiener type and was constructed to minimize the contribution from the cosmological signal in the filtered maps in the presence of noise, \mathcal{N} , i.e. it minimizes $\langle (\Delta T - \mathcal{N})^2 \rangle$ (Kashlinsky et al 2009). In ℓ -space the filter is given by

$$F_{\ell}^{\text{KAB}} = \frac{C_{\ell}^{\text{sky}} - C_{\ell}^{\Lambda\text{CDM}} B_{\ell}^2}{C_{\ell}^{\text{sky}}}, \quad (4)$$

where C_{ℓ}^{sky} is the actual realization of the radiation power spectrum in the sky that includes noise, TSZ, KSZ, foreground residuals, and primary CMB; $C_{\ell}^{\Lambda\text{CDM}}$ is the power spectrum of the ΛCDM model that best fits the data, and B_{ℓ} is the antenna beam for a given DA. Since the quadrupole and octupole are aligned with the dipole, the KAB filter is set to zero for $\ell \leq 3$ to avoid any cross-talk from the corresponding large angular scales that could mimic a dipole. In Fig. 3a we represent the KAB filter for the W1 DA. The filter has structure at all multipoles and is therefore sensitive to KSZ power across the full multipole range.

2.3. OMCP filters.

OMCP used Matched Filters (MF), i.e., filters that are suited to distinguish point sources from a background signal, provided the profile of the source is known. In their analysis, OMCP assumed that all clusters are unresolved and approximated their profiles by the WMAP beam function. In ℓ -space this means

$$F_{\ell}^{\text{OMCP}} = \frac{B_{\ell}}{(C_{\ell}^{\Lambda\text{CDM}} + C_{\ell}^{\text{TSZ}})B_{\ell}^2 + N_{\ell}}, \quad (5)$$

where C_{ℓ}^{TSZ} and N_{ℓ} are the power spectrum of the TSZ effect and of the white and homogeneous instrumental noise, respectively. B_{ℓ} is the antenna beam. In addition, OMCP considered clusters to be isothermal, in which case the TSZ and KSZ profiles are proportional to each other. By measuring the TSZ component in the original and in the filtered data, the fraction of the KSZ lost due to filtering could be computed exactly. However, since clusters are *not* isothermal (as demonstrated, e.g., by Atrio-Barandela et al. 2008), their electron-density and pressure profiles are in fact different, causing filters that disregard this fact to potentially suppress the KSZ signal relative to the TSZ contribution. In Fig. 3b we plot the OMCP filters for eight WMAP DAs, corresponding to the Q (dot-dashed green line), V (dashed blue) and W (solid red) bands. These filters are effectively band-pass filters, removing all power below $\ell \sim 200 - 300$ and above $\ell \sim 800 - 1000$.

OMCP also considered a modified MF, named Unbiased Multifrequency Matched Filter (UF), designed to remove the TSZ contribution. Since this second filter was found to be even less sensitive to bulk flows than MF, we will not consider it further. Our approach to reducing any TSZ contamination will be the same for all filters, namely to compute dipoles at the zero-monopole aperture.

2.4. The Mody-Hajian filter.

MH used a Wiener filter designed to remove the TSZ and instrument noise contributions together with the intrinsic CMB, leaving only the KSZ component in the data. Their filter is defined by

$$F_{\ell}^{\text{MH}} = \frac{C_{\ell}^{\text{KSZ}} B_{\ell}^2}{[C_{\ell}^{\Lambda\text{CDM}} + C_{\ell}^{\text{TSZ}}] B_{\ell}^2 + N_{\ell}}, \quad (6)$$

where C_{ℓ}^{KSZ} is the power spectrum of the KSZ contribution, and the other terms have the same meaning as in eqs. (4, 5). This filter neglects the inhomogeneities in the instrumental noise and assumes that C_{ℓ}^{KSZ} , the quantity to be measured, is known. To construct their filter, MH need to 1) specify the cluster distribution on the sky, 2) assume an electron density profile for all clusters, and 3) fix the cluster extent, all quantities that have yet to be measured from the data. In Fig. 3c we plot the MH filter for assumed cluster extents of $10'$ and $15'$; both are convolved with the beam of the W1 DA. The filter is normalized to a KSZ dipole in the Z-direction with an amplitude of $10\mu\text{K}$; convolution with the beam reduces the amplitude to $\sim 5\mu\text{K}$. The resulting two curves can be thought of as two extreme cases of what the actual MH filter might be. Taking into account that very few clusters are resolved in the WMAP W band, we will in the subsequent discussion only consider the MH filter constructed assuming an angular radius of $10'$.

2.5. Cluster apertures on the filtered data.

Filtering not only removes the intrinsic CMB component, it also modifies the KSZ signal, affecting the cluster extent and its electron density profile. To evaluate the monopole and dipole at N_{cl} cluster positions on the sky we first need to discuss what would be the radial extent of each cluster in the filtered data. In Kashlinsky et al (2008) we considered that clusters extended 4–6 times the radial extent of the region emitting 99% the total X-ray flux. Since Kashlinsky et al. (2010) we quote instead the dipole evaluated on discs of $\sim 25'$ aperture radius, the same size for all clusters. In both cases, the monopole was close to zero and the measured dipole did not differ significantly. *Evaluating dipoles at the zero monopole aperture is crucial to guarantee that the measured dipole has no significant contribution from the TSZ effect:* since the monopole is dominated by the TSZ contribution, the amplitude of the former is an upper limit to any dipole due to the inhomogeneous distribution of clusters on the sky.

The cluster profile, $T(\theta) = (1/4\pi) \sum (2\ell + 1) T_{\ell} P_{\ell}(\cos\theta)$, when convolved with the antenna beam B_{ℓ} and the filter F_{ℓ} , becomes:

$$(F \star T)(\alpha) = A \sum (2\ell + 1) F_{\ell} T_{\ell} B_{\ell} P_{\ell}(\cos\alpha), \quad (7)$$

where A is a normalization constant. In Figs. 3d–f we plot the filter profile in real space of the W-band (solid red lines). This would be the cluster profile in the filtered map if it were a Dirac δ -function, i.e., if the cluster was unresolved. For comparison, the dashed line represents Gaussian beam with the resolution of the W band.

To assess the impact of the aperture choice, we compute the measured cluster profile from eq. (7), averaged over a disc of angular radius ρ , as it was done in the data

$$\langle F \star T \rangle_{\rho} = \frac{1}{\rho^2} \int_0^{\rho} [(F \star T)(\alpha)] d \cos \alpha. \quad (8)$$

In Fig. 3g–h we plot the above average vs the angular radius ρ of the disc for the KAB, OMCP, and MH filters, respectively. To avoid overcrowding the plots, we only show the Q1, V1 and W1 DAs. For the KAB filter the signal

vanishes around $20'$, while it extends to $30'$ for the OMCP filters, and well beyond $40'$ for the MH filter. These radial extents correspond to unresolved clusters; for real sources the signal will spread to apertures of even *larger* radii. Empirically, we found that the zero monopole aperture was around $25'$ for the KAB filter, whereas slightly above $20'$ would correspond to all clusters being unresolved by the antenna beam. The zero monopole defines a physically well motivated aperture over which to compute the dipole. *This point was missed by OMCP and MH, who never have addressed this issue.*

2.6. Summary of previous results.

The filters discussed in this section are spherically symmetric. They cannot imprint a dipole at zero monopole exclusively at cluster locations on a filtered map but, if not carefully designed and implemented, they can erase it to below the statistically significant level. OMCP implemented two matched filters, named MF, described in Sec. 2.3, and UF. They measured the dipole at the position of 736 clusters of galaxies and found no significant KSZ signal. OMCP tested the performance of their filters using simulated maps and showed that their filters begin to recover the input velocity only at speeds $V_{\text{bulk}} \simeq 4,000 \text{ km s}^{-1}$ for the MF and $V_{\text{bulk}} \simeq 10^4 \text{ km s}^{-1}$ for the UF. The average mean optical depth of the clusters in their sample is quoted as $\langle \tau \rangle \simeq 4.9 \times 10^{-3}$ (Sec. 4.5 of OMCP), and the resulting temperature anisotropy would be $\Delta T = 183 \mu\text{K} (\tau/0.005) (V_{\text{bulk}}/4000 \text{ km s}^{-1})$. Velocities approaching or exceeding $4,000 \text{ km s}^{-1}$ thus induce anisotropies that would be measurable in the original data and for each individual cluster, without any need for filtering.

The root cause of this problem is that OMCP's implementation of their filters did not increase the S/N but strongly reduced it, to the extent of rendering their filters unable to detect a CMB dipole corresponding to a bulk-flow velocity of $\sim 600 - 1000 \text{ km s}^{-1}$. The poor performance of their filters is also due to the fact that OMCP effectively measured the dipole only at the central cluster pixels because their filters were optimized to reconstruct the source amplitude if the source was centered on that pixel (Mak et al 2011). Since clusters in the filtered maps reach a zero monopole aperture at $\sim 30\text{-}40'$ (see Fig. 3d-i) the implementation by these authors does not use all the information available in the filtered map. Also, OMCP assumed that the KSZ and TSZ cluster profiles are identical and unresolved. However, any filter that efficiently removes the TSZ signal will also remove a substantial part of the KSZ signal. This is the reason why the better designed UF requires three times larger velocities than the MF to detect the average motion of ~ 700 clusters.

MH, by contrast, used a different approach. Instead of computing the dipole at the locations of clusters, MH fit dipole templates to their filtered maps. This approach is flawed in two important respects: (a) MH require that the total number of clusters, their profiles, and extents be known in advance in order to construct their filter, and (b) by matching the same cluster template to the filtered data MH implicitly assume that all clusters have the same profile and extent in the sky as in the filtered CMB data. Hence, changing the profile, number, or extent of clusters changes the filter (and the filtered map) and the final results. As both OMCP and MH restricted their analyses to apertures smaller than the ones used by KABKE, the dipole measured by us could have remained undetected in the residual CMB and noise of their filtered maps.

3. MEASURING BULK FLOWS IN WMAP DATA WITH THE KAB METHOD.

To measure the dipole at the locations of clusters in CMB maps filtered following KAB, OMCP, and MH, our pipeline proceeds as follows:

1. For each DA, the data are multiplied by the extended mask KQ75 for the WMAP7 data release. Then, monopole, dipole, and quadrupole are subtracted from the regions outside the mask. Next, we compute the multipole expansion coefficients $a_{\ell m}$. The power lost due to masking is corrected for by multiplying each multipole by $f_{\text{sky}}^{-1/2}$, where f_{sky} is the fraction of the sky outside the mask.
2. The $a_{\ell m}$ coefficients are multiplied by the filter F_{ℓ} before transforming them back into real space to create the filtered map.
3. The monopole and dipole outside the mask are removed from the filtered maps.
4. Dipoles are computed at the cluster positions using the same aperture of radius ρ for all clusters. We repeat the measurement for different ρ and, as indicated in Sec. 2.5, we select the dipole measured at the *zero monopole* aperture.

To translate the measured dipole amplitude from temperature units to velocity units, we need to compute how the mean cluster opacity changes with filtering. Owing to the different functional form of the three filters, they will affect the KSZ power differently. Since $\tau = \tau(\theta)$, to compute the average $\langle \tau \rangle$ over our cluster sample we need the electron density profile and of the cluster radial extent of all clusters, information that is not presently available. In the KAB filter, this uncertainty translates into a calibration uncertainty but does not affect the amplitude of the dipole in μK nor its direction. As discussed, this uncertainty is built into the definition of the OMCP and MH filters. In order to facilitate the comparison of the results obtained with the different filtering schemes, we will use the results presented in Figs. 3d-f to normalize the filtered maps as described below.

Cluster Sample	N_{cl}	$\langle\Delta T\rangle[5']/\mu\text{K}$				$R^F\langle\Delta T\rangle[30']/\mu\text{K}$		
		WMAP	KAB	OMCP	MH	KAB	OMCP	MH
I $0.5 < L_X < 1$	208	-14 ± 9	-4 ± 7	-24 ± 26	-0.03 ± 0.01	-1.5 ± 0.9	-2.3 ± 1.0	-8.3 ± 1.9
II $1 < L_X < 2$	179	-21 ± 7	-10 ± 8	-50 ± 28	-0.02 ± 0.008	2.4 ± 0.7	-0.8 ± 0.9	-1.9 ± 1.5
III $L_X > 2$	119	-40 ± 10	-30 ± 5	-138 ± 40	-0.09 ± 0.02	1.0 ± 1.5	-4.2 ± 1.3	-13 ± 2

TABLE 1

DIFFERENT CLUSTER SAMPLES CONSIDERED IN THIS WORK AND SOME OF THEIR PROPERTIES. N_{cl} IS THE NUMBER OF CLUSTERS IN EACH SUBSAMPLE AND X-RAY LUMINOSITIES ARE GIVEN IN UNITS OF 10^{44} ERG S $^{-1}$.

3.1. Filter normalization and filtered maps.

The filters defined in Sec. 2 and depicted in Fig. 3a-c do not only differ in shape but also in normalization. To normalize a map we need to derive a coefficient R^F that measures how much the dipole is diluted by the filter. If $\tau(\theta)$ and $F \star \tau(\theta)$ are the cluster optical depth in the unfiltered and filtered maps, then the normalization coefficient would be $R_F = \langle\tau\rangle/\langle F \star \tau\rangle$, where the average is taken over the solid angle subtended by the clusters in unfiltered and filtered data. This parameter is not simple to compute since both profiles and angular extents are unknown. Instead, an approximated normalization coefficient can be computed by taking into account that relaxed clusters are close to isothermal in their central regions (Pratt et al. 2011) and electron pressure and electron density are proportional to each other. Hence, in those regions *filtering would dilute the TSZ and KSZ signal in the same proportion*. Then, $R^F \approx \langle\Delta T_{TSZ}\rangle_\rho / \langle F \star \Delta T_{TSZ}\rangle_\rho$ where the average is on a small disc of radius ρ around the cluster center in both the unfiltered and filtered maps. In Table 1 we list the monopole as measured within an aperture of $5'$ radius in the original WMAP data and in the KAB, OMCP, and MH filtered maps. The quoted values correspond to the mean and rms dispersion of the four W DAs. We divide our sample according to X-ray luminosity in three independent bins to test the correlation of our measurements with X-ray luminosity as in Kashlinsky et al (2010). Within $5'$ the measured R^F is rather uncertain since the temperature anisotropy contains CMB residuals and noise together with TSZ. This is specially evident for the less massive clusters (sample I). From Table 1, the renormalization coefficient is ~ 2 for the KAB filter, ~ 600 for the MH filter whereas the OMCP filter does not dilute but boosts the signal (but not the S/N) by about a factor of 3. Since all clusters in our sample have been fit to a β -model, we can use this profile to compute numerically R^F . It should be computed separately for each cluster sample and DA. Nevertheless, *to avoid introducing an extra variance, we will use the same values of R^F for all cluster configurations and bands*. In this way, we do not change the S/N ratio of the measured dipoles when expressed in μK . For the full sample the ratios are $R^F \simeq [1.7, 0.37, 530]$ for the KAB, OMCP and MH filters, respectively. Since different bands have different normalization coefficients and different zero monopole aperture, we concentrate our study on the 4 DAs of the W-band. Although the results averaged over all WMAP bands are very similar due to the noise, by using only the W-band, the statistical significance of the measured dipole is slightly decreased. For the purpose of this paper this is not important since we are only interested in comparing the S/N ratio of the three filters.

Our normalization is useful for comparing the results of different filters since all filtered maps have similar power. It enables us to subtract maps from each other to compare their different structure. In Fig. 4 (left column) we show the KAB, OMCP, and MH filtered maps of the W1 DA. The KAB map exhibits more structure on large scales since our filter preserves power below $\ell = 300$. The OMCP filter erases all power at $\ell \lesssim 200-300$, and hence the resulting filtered maps show no large-scale features. The MH filter, finally, preserves power over a wide range of scales ($50 \lesssim \ell \lesssim 600$) but not on the largest scales. Consequently, the MH filtered map shows pronounced structure only on intermediate scales. The differences in the impact the filters have on the CMB signal become clearer when the filtered maps are subtracted from each other. The subtracted maps are shown in the right column of Fig. 4. As expected, the difference between the KAB and OMCP maps is most prominent on large angular scales. The differences between the OMCP and MH filtered maps are dominated by features on intermediate scales to which the MH filter is sensitive, whereas the OMCP filter is not. The difference between the KAB and MH maps, finally, exhibits a more complex pattern that combines the effects of the KAB filter's sensitivity to very low multipoles (large scales) and the MH filter's emphasis on intermediate scales (cf. Fig. 3).

3.2. Cluster-by-cluster comparison of the filtering schemes

Any meaningful filter should significantly remove the primary CMB component or else it would not be able to isolate the much smaller KSZ dipole term lurking beneath it. The TSZ component also needs to be lowered. Filters redistribute differently the power of the intrinsic CMB anisotropies, TSZ and KSZ. Before discussing the efficiency of each filter we investigate empirically how each of the filtering schemes transfers the TSZ and primary CMB components with CMB temperature, averaged over apertures of size $\rho = 10'$ $20'$ and $30'$, at each cluster location \hat{n}_j on the sky, $\langle\Delta T(\hat{n}_j)\rangle_\rho$. The all-sky mean of all $\langle\Delta T\rangle$ is the monopole that we use to define the zero-monopole aperture. We will illustrate our findings with the W1 DA data which has the best angular resolution. By choosing the data at the same DA, we make sure that all three datasets have the same instrument noise realization on a per pixel basis.

In Fig. 5 we plot the mean temperature anisotropy in the central parts of all the clusters in our sample III of Table 1, corresponding to the aperture radius $\rho = 10'$, comparing the OMCP- and MH-filtered maps with the KAB-filtered data. The figure shows that on average the same CMB components, i.e. the primary CMB and TSZ that are present in the central parts of clusters in the KAB-filtered maps, are also present in the other two filtered maps. At the same

Filter	$\sigma_0/\mu\text{K}$	$D_X/\mu\text{K}$	$D_Y/\mu\text{K}$	$D_Z/\mu\text{K}$	$D/\mu\text{K}$	$l/1^\circ$	$b/1^\circ$
KAB	30	-3.0 ± 2.7	-5.5 ± 2.4	1.8 ± 2.0	6.5 ± 2.3	241 ± 27	16 ± 18
OMCP	23	-0.7 ± 2.0	-2.0 ± 1.8	1.2 ± 1.5	2.4 ± 1.4	251 ± 67	30 ± 28
MH	67	-2.6 ± 5.7	-7.0 ± 5.3	4.1 ± 4.4	8.5 ± 4.4	249 ± 57	29 ± 26

TABLE 2
DIPOLE COMPONENTS, MODULI AND DIRECTIONS FOR THE THREE FILTERS.

time, there are also notable differences which manifest themselves in the dispersion shown in the plot. The dispersion of the MH- vs KAB-filtered data is much larger than in the OMCP vs the KAB case. The correlation coefficient between KAB and OMCP is 0.94 dropping to only 0.62 for KAB and MH. This comparison shows empirically that the filters redistribute the profile (and each of the components) very differently.

The primary CMB and TSZ components present at $\rho = 10'$ need to be removed if there is any hope of detecting the KSZ-like dipole. Fig. 6 compares the mean temperature over $\rho = 20'$ and $30'$ with that at $\rho = 10'$ for the W1 DA in two redshift bins of roughly the same number of clusters. Fig. 6a-c correspond to our samples II and III, and Fig. 6d-f to clusters in our sample not considered in this study. The plots illustrate empirically that KAB removes the intervening components better than the other two filters. For the KAB filter, there is little to no correlations at these larger radii with the central part, consistent with this filter having removed the components present at $10'$, *the main obstacle to measuring the KSZ-like dipole*. The OMCP filter (middle panels) shows the presence of these components at the $\rho > 20'$ aperture radii and thus it is not as efficient as the KAB filter. The MH filter performance is much more dismal; it shows an almost perfect correlation between the larger apertures and that at $10'$, implying that the same components that have prevented the measurement of the KSZ signal in cluster centers remain, although redistributed, as far out as $\rho > 30'$.

3.3. Dipoles.

To compare the performance of the three filters, we computed dipoles for each filter and for the three cluster samples of Table 1. We used the following apertures of radius $\rho = [5, 10, 20, 30, 40, 50, 60]$ arcmin in order to select a suitable zero-monopole aperture for each filter. As indicated, all data are renormalized by multiplying the filtered KAB, OMCP and MH maps by the coefficients $R^F = [1.7, 0.37, 530]$, respectively. With this normalization, the monopole evaluated on apertures of $5'$ would have the same amplitude in the three filtered maps. Ideally, this would also be true for the dipole. By using a single coefficient, the S/N of the dipole measurement in each cluster configuration remains unaltered.

In Table 1 we also list the value of the monopole residual at $30'$ in the renormalized maps. The KAB zero monopole aperture occurs at $\leq 30'$ radius, for OMCP is at $\sim 30'$ - $40'$ and for MH is at $\geq 50'$; Table 1 shows that at $30'$ the MH filter still contains non-zero monopole residuals, in agreement with Fig. 6. In Figs. 7a-c we plot the three components (X,Y,Z) of the dipoles measured with an aperture of $30'$ versus the TSZ monopole at $10'$ radius. In Fig. 7d we plot the dipole moduli. The three cluster subsamples of Table 1 are represented with the same symbol. They can be easily distinguished since the average TSZ monopole increases with increasing X-ray luminosity. Notice that each cluster subsample has similar monopoles at $10'$ for the three filters as expected since our normalization was constructed to produce the same TSZ amplitude in the central parts of clusters at $5'$.

The errors on the measured dipoles σ_i , $i = (X, Y, Z)$, were obtained from the dispersion of dipoles measured in random cluster positions in the sky. For each component, the error scales approximately as (Atrio-Barandela et al 2010)

$$\sigma_i^2 = \frac{(\sigma_i^{\text{res CMB}})^2}{N_{\text{cl}}} + \frac{(\sigma^{\text{noise}})^2}{N_{\text{pix}}N_{\text{DA}}} \quad (9)$$

where $\sigma_i^{\text{res CMB}}$ is the rms dispersion of the CMB residual in the filtered map, σ^{noise} the dispersion of the noise, N_{pix} the number of pixels occupied by the cluster sample and N_{DA} the number of DAs used in the analysis. We considered four cluster samples with different numbers of clusters (100, 200, 400 and 800 clusters). For each sample, we generated 4,000 random cluster distributions. If clusters sampled the sky homogeneously then the error on the monopole, σ_0 , and in each dipole component would be related by $\sigma_i = \sqrt{3}\sigma_0$. For an inhomogeneous cluster distribution the relation is given by $\sigma_i \simeq \sigma_0/\langle n_i^2 \rangle^{1/2}$ where $\langle n_i^2 \rangle$ is the average of the direction cosines of the clusters in the sample (Atrio-Barandela et al. 2010, Atrio-Barandela 2013). Since the Galaxy removes a large fraction of the sky, preferentially in the X direction, errors are larger for D_X than for D_Y or D_Z . We verified that this was the case for the three filters, being 10-18% and 2-3% larger with respect to a homogeneous distribution of clusters for X and Y, respectively, and a 15% smaller for Z. Since the errors are dominated by the residual CMB, they scale as $N_{\text{cl}}^{1/2}$, as dictated by eq. (9). For each cluster sample, the error on each dipole component is scaled by the number of clusters from the error obtained on the simulations. The errors on the modulus of Fig. 7d were obtained from the rms dispersion of 10,000 dipoles. Those dipoles were generated by adding to the each measured dipole component a random value drawn from a gaussian distribution with zero mean and dispersion σ_i .

The results from the three filters show a reassuring degree of consistency regarding the value of the Y-component of the dipole. This component is always negative for all filters and all cluster configurations, in agreement with the DF results, which combine a pronounced negative Y-component with a positive Z-component of lower amplitude and an

X-component that is consistent with zero within the measurement uncertainties. The KAB filter (blue filled circles) shows a very clear correlation of the Y dipole component with the monopole at $10'$ (Fig. 7b) and so does the overall dipole amplitude (Fig. 7d). This correlation is found at $30'$, when the TSZ monopole is zero. Then, there can not be a TSZ dipole contribution due to an inhomogeneous cluster distribution. It is instructive to revisit Fig. 6a: cluster by cluster, the average temperature anisotropy on a disc of $10'$ is uncorrelated with the same average over a disc of $30'$.

Fig. 7a also shows a strong correlation for X-component in the MH filter (green triangles). However, in this case we expect this correlation to be due to the TSZ effect. As our error analysis show, the X-component of the dipole is the worst measured since the Galaxy is most predominant in this direction. Then, one has to expect an important TSZ dipole due to the inhomogeneous distribution of clusters in the sky in agreement with the fact that for the brightest clusters, sample III, the residual TSZ monopole at $30'$ is $\langle \Delta T(30') \rangle = -13 \pm 2 \mu\text{K}$, large in comparison with the value of the other two filters (see Table 1). It is also in agreement with the result of Fig. 6c that shows that the average temperature anisotropy at cluster locations within discs of radius $30'$ (TSZ monopole) is strongly correlated with the same average at $10'$ and, consequently, so it would be the TSZ dipole at $30'$. We verified that the measured dipoles are in fact very small at the $50'$ aperture, the zero monopole aperture for this filter.

With respect to the OMCP filter (open red squares) the dipole is always small and shows no correlation with the monopole at $10'$. The low dipole amplitudes were to be expected since this filter cuts off all the power at multipoles $\ell \leq 300$ (compare Fig. 2b and Fig. 3b) and therefore is insensitive to half the dipole signal. At this filter zero monopole aperture, $\sim 40'$ the results were not very different, showing no significant dipole either.

3.4. Consistency of the measured dipoles.

Since the three cluster samples of Table 1 are independent the motion of all the clusters can be obtained by averaging the measured dipoles $D_{i,s}$ in each sample $s = (I, II, III)$ weighted by their respective errors $\sigma_{i,s}$

$$D_i = \left(\sum_s D_{i,s} / \sigma_{i,s}^2 \right) / \left(\sum_s 1 / \sigma_{i,s}^2 \right) \quad (10)$$

In Table 2 we give the resulting dipoles for the three filters. We also give σ_0 , the rms dispersion of the monopole. Consistently, the error bars on the dipoles are $\sigma_{(X,Y,Z)} \simeq \sigma_0 \sqrt{3/N_{cl}}$, being larger for the X and smaller for the Z components, as we found with the simulated dipoles (see Sec 3.3). In the table we also give the dipole amplitude and direction for the three filters. The errors were computed from the dispersion of 10,000 dipole moduli and directions as in Fig 7d. Notice the remarkable agreement between the direction of the three filters. The angular separation between the central value of the direction of the KAB filter and that of OMCP and MH is about 16° . More remarkable is the close alignment between the direction of the OMCP and MH dipoles. However, the errors on the direction are large and we can not derive a final conclusion of this coincidence since the MH dipoles have probably an important contamination from the TSZ monopole, as discussed in Sec 3.3.

The results of Table 2 are crucial to understand the performance of each filter. Of the three filters, the KAB filter has the largest S/N. By effectively removing all multipoles with $\ell \leq 300$, OMCP filtered maps contain a small fraction of CMB residuals and give the smallest error bars. Unfortunately, the filter is also very effective in removing the dipole signal, degrading the overall S/N. Thus, our results agree with the original OMCP analysis since velocities above $4,000 \text{ km/s}$ were required on samples of ~ 700 clusters for the dipole to be detectable. By comparison, the MH filter measures dipoles of larger amplitude but the error bars are also large. Only the KAB filter provides statistically significant result. For this cluster sample our measurement is significant at the 93% confidence level, smaller than in Kashlinsky et al (2010) (see Atrio-Barandela et al, 2013, for a full discussion) while the results of the OMCP and MH have a significance below 60%, reflecting the poor performance of these two filters.

3.5. From temperature to velocity.

To compare properly the results of the different filters, dipoles need to be expressed in velocity and not in temperature units. In Kashlinsky et al (2009) we denoted the calibration coefficient as: $C_{1,100} = (D/V_{\text{Bulk}}) = (T_0/c) \langle F \star \tau \rangle$, with D the dipole in μK and $\langle F \star \tau \rangle$ the *filtered* cluster profile averaged solid angle subtended by the cluster population. For the correct profile, $V_{\text{Bulk}} = D/C_{1,100}$ would be independent of the aperture used to measure the dipole. To account for the dilution effect introduced by the filter our filtered maps have been renormalized by R^F (see Sec 3.1). In the renormalized maps, $C_{1,100} = (T_0/c) \langle \tau \rangle$. Using the β model data, we can compute $\langle \tau \rangle$ for our cluster sample for different apertures. We find that for $\rho = 5, 10, 15'$, the coefficient averaged over the four W DAs is $C_{1,100} = (1.36 \pm 0.08, 1.07 \pm 0.05, 0.86 \pm 0.03) [\mu\text{K}/100 \text{ km s}^{-1}]$, respectively. Since Fig. 5 shows that at the $10'$ aperture the three renormalized filtered maps have similar monopoles at the cluster locations, we can assume that $\langle \tau \rangle$ is also similar for the three filters out to that aperture. Then, by taking the conversion factor for $10'$ we can translate the dipole into a velocity

$$V_{\text{Bulk}}^{\text{KAB}} = 607 \pm 215 \text{ km s}^{-1}, \quad V_{\text{Bulk}}^{\text{OMCP}} = 224 \pm 131 \text{ km s}^{-1}, \quad V_{\text{Bulk}}^{\text{MH}} = 794 \pm 411 \text{ km s}^{-1}. \quad (11)$$

With this normalization, the dipole amplitude in km s^{-1} is lower than the value of $\sim 1000 \text{ km s}^{-1}$ found previously (see Kashlinsky et al 2009, 2011 for a full discussion on our previous method). Nevertheless, our calibration of the flow is still not exact since the β model is not an accurate description of cluster profiles outside the X-ray emitting inner part. The dipole is measured at $30'$ while $C_{1,100}$ is computed at $10'$. If $C_{1,100}$ is smaller at $30'$, as suggested by the

calculation at $15'$, then the corresponding velocities will be larger. For instance, if $C_{1,100} \sim 0.55[\mu\text{K}/100\text{kms}^{-1}]$ then the velocities will be those of our previous work.

Even if our calibration of the flow is still uncertain due to lack of proper data, it does not affect the statistical significance of the dipole measured with any of the three filters. The KAB filter does not only measures a dipole that correlates with cluster X-ray luminosity; it provides the largest signal to noise ratio of the three filters discussed here. Nevertheless, the discrepancies between the three filters could be real if the three filters are probing the flow at different scales. For instance, since the OMCP filter is sensitive primarily to scales corresponding to $\ell \geq 300$, it gives all the weight to unresolved clusters which are, on average, farther away. By contrast, the KAB dipole includes contributions from nearby systems, owing to the filter's greater sensitivity to low multipoles. While some degree of discrepancy between filters could simply reflect spatial variations in the properties of the flow, the fact is that none of the filters but KAB has been shown to be limited by cosmic variance, has provided a statistically significant measurement or has shown a correlation with X-ray luminosity at the zero monopole aperture. Therefore, the results obtained using the OMCP or MH filters can not be interpreted as ruling out any possible large scale flow detected by the KAB filter.

4. SUMMARY AND CONCLUSIONS.

We can now proceed with the summary of the appropriateness of the three filtering schemes in uncovering the KSZ-like dipole signal in the KAB method.

- **KAB filter.** This filter is the most appropriate of the three as has already been explained in the original KAB paper. It removes the primary CMB down to the fundamental limit imposed by the cosmic variance as demonstrated analytically and numerically in Atrio-Barandela et al (2010). It has the smallest zero monopole aperture of the three filters and, as Fig. 6 shows, at the final - zero monopole - aperture the CMB does not correlate in any meaningful manner with that at the central parts. This therefore allows to look for the KSZ dipole component after the TSZ has been made vanishingly small because of the cluster X-ray temperature decrease toward the outer parts (Kashlinsky et al 2009). The dipole uncovered at cluster positions at such aperture contains a negligible TSZ component, which dominates the central parts at $\rho = 10'$. The filter is sensitive to a KSZ dipole spread over the whole ℓ space and shows the largest S/N of all the filters analyzed here.
- **OMCP filter** is clearly not as efficient as the KAB. By cutting power at $\ell \leq 300$ it reduces the residual CMB that dominates the error bar but also decreases the signal, reducing the overall S/N of the filter. This point was already demonstrated implicitly in Fig. 13 of OMCP which shows that no bulk flow can be reliably measured with this filter at velocities $< 4,000 - 10,000$ km/sec; we find it strange that, given those numbers, claims are occasionally still made about the alleged efficiency of this filter. Fig. 6 and Table 2 demonstrate explicitly that if one uses this filter, particular care must be made to work at the appropriately large apertures of at least $> 30'$ in radius. Nevertheless, as the filter is only sensitive to a rather small range of multipoles ($\ell \geq 300$), even at these large apertures the signal has been erased as to make the dipole undetectable.
- **MH filter.** This filter is the least useful for the application to the KAB method. Even at apertures as large as $> 30'$ it still leaves primary CMB and TSZ components, as demonstrated by the clear correlation in Fig. 6c, that confuse any determination of the KSZ-like dipole signal. Furthermore, the filter does detect a dipole at the $30'$ aperture, but due to the large monopole residuals, there exists important contributions due to TSZ dipoles. The measured dipoles have the largest error bars and, like in the OMCP filter, the results are not statistically significant.

To conclude, we have compared the dipoles measured at the locations of X-ray selected galaxy clusters using the filters proposed by OMCP and MH with the results obtained with the KAB filter. *We find that all filters recover dipoles; the central values of the directions are aligned but the KAB dipole is the most efficient since it has the largest statistical significance.* The discrepancy between these findings of ours and the results published by OMCP and MH is due to the latter teams failing to chose the right aperture for their measurement. In addition, their simulations and calibrations assume the same profile for the electron density and electron pressure, hypothesis that is bound to degrade their filter performances if real clusters are not described by their profiles.

In comparison with the other filters, the KAB filter makes no assumptions about cluster profiles or extents, and by design removes the intrinsic CMB, the largest contaminant (see eq. 1) down to the limits imposed by cosmic variance. The impact of all uncertainties associated with our limited knowledge of the cluster profile and extent is limited to a single normalization coefficient $C_{1,100}$ that does not affect the filter definition. In addition, the zero-monopole aperture for the KAB filter has a radius of $\lesssim 30'$, smaller than what is required by the other two filters. Finally, the dipole signal recovered with the KAB filter is strongly correlated with the central TSZ monopole (or the equivalent X-ray luminosity, Kashlinsky et al 2010), a clear indication that the dipole is not produced by some random contribution of the residual CMB. These three aspects make the KAB filter the least affected by possible systematics among the filters suggested to date. Alternative filtering schemes can possibly be designed, but their design must ensure that they increase the S/N of the measurement, not decrease it. Finally, filters redistribute the information from real to filtered space by weighing angular scales differently. Therefore, they are probing the velocity field on different scales and the discrepancies on modulus and direction could reflect the spatial variations of the flow. To demonstrate that filters probe the same or different flows would require accurate cluster profiles and it goes beyond the scope of the present work.

Recently, and well after this paper had been submitted to peer-review, the Planck Collaboration carried out the analysis of the filters described here using the recently released Planck data (Planck Intermediate Result XIII, Planck Collaboration, 2013). The KSZ team analyzed peculiar velocities using the Internal Linear Combination (ILC) map, constructed by combining data at different frequencies with varying weights in ℓ -space in order to reduce the foreground contribution. The results found using the KAB filter were in agreement with ours but the Planck Collaboration assigned larger statistical uncertainties, reducing their statistical significance. The flaws of their analysis, that lead to an overestimation of their errors, are discussed in Atrio-Barandela (2013). Also, the ILC data is not the best suited data for this analysis. Since the weights of different frequencies vary with ℓ , the power of the SZ signal is scrambled across different multipoles and makes it very difficult to establish how filters that operate on ℓ -space transfer the cluster signal. Peculiar velocity measurements will be better studied using Planck frequency data. Frequency information will be critical to establish the origin, nature, and scale of the dipole measured in the WMAP data. Cluster profiles can be measured individually to determine the effect of filtering on each of the clusters; the frequency coverage would be crucial to remove any TSZ dipole component and, specifically, the 217 GHz channel would be important to test for systematics.

FAB acknowledges financial support from the Spanish Ministerio de Educación y Ciencia (grants FIS2009-07238, FIS2012-30926 and CSD 2007-00050). HE gratefully acknowledges funding provided by NASA grant NNX10AJ69G.

REFERENCES

- Atrio-Barandela, F., Kashlinsky, A., Kocevski, D. & Ebeling, H. 2008, *ApJ*, 675, L57
- Atrio-Barandela, F., Kashlinsky, A., Ebeling, H., Kocevski, D., Edge, A. 2010, *ApJ*, 719, 77
- Atrio-Barandela, F. 2013, *A&A*, 557, A116
- Birkinshaw, M. 1999, *Phys. Rep.*, 310, 97
- Böhringer, H., et al. 2004, *A&A*, 425, 367
- Cavaliere, A. & Fusco-Femiano, R. (1976) *A&A*, 49, 137
- Ebeling, H., Mullis, C. R., & Tully, R. B. 2002, *ApJ*, 580, 774
- Ebeling, H., et al. 1998, *MNRAS*, 301, 881
- Ebeling, H., et al. 2000, *MNRAS*, 318, 333
- Gorski, K. et al 2005, *ApJ*, 622, 759
- Haenhelt, M. G., & Tegmark, M. 1996, *MNRAS*, 279, 545
- Kashlinsky, A. & Atrio-Barandela, F. 2000, *Astrophys. J.*, 536, L67 (KAB)
- Kashlinsky, A., Atrio-Barandela, F., Kocevski, D. & Ebeling, H. 2008, *ApJ*, 686, L49 (KABKE)
- Kashlinsky, A., Atrio-Barandela, F., Kocevski, D. & Ebeling, H. 2009, *ApJ*, 691, 1479
- Kashlinsky, A., Atrio-Barandela, F., Ebeling, H., Edge, A., & Kocevski, D. 2010, *ApJ*, 712, L81
- Kashlinsky, A., Atrio-Barandela, F. & Ebeling, H. 2011, *ApJ*, 732, 1
- Kashlinsky, A., Atrio-Barandela, F., Ebeling, H. 2012, *Phys. Rep.* (submitted). Preprint: arXiv:1202.0717
- Kocevski, D. D., et al. 2007, *ApJ*, 662, 224
- Keisler, R. 2009, *ApJ*, 707, L42
- Komatsu, E., & Seljak, U. 2001, *MNRAS*, 1353
- Mak, D. S. Y., Pierpaoli, E., & Osborne, S. J. 2011, *ApJ*, 736, 116
- Mody, K. & Hajian, A. 2012, *ApJ*, 758, 4 (MH)
- Osborne, S. J., Mak, D. S. Y., Church, S. E., & Pierpaoli, E. 2011, *ApJ*, 737, 98 (OMCP)
- Planck Collaboration. Planck Early Results XXVI, 2011, *A&A*, 536, 26
- Planck Collaboration. Planck Early Results: The all-sky early Sunyaev-Zel'dovich cluster sample, 2011, *A&A*, submitted. Preprint, 1101.2024.
- Planck Collaboration. Planck Intermediate Results V, 2012, *A&A*, submitted. Preprint arXiv:1207.4061
- Planck Collaboration. Planck Intermediate Results XIII: Constraints on Peculiar Velocities, 2013, *A&A*, submitted. Preprint arXiv:1303.5090
- Pratt, G. et al. 2011, *A&A*, 461, 71
- Sunyaev, R. A. & Zel'dovich, Y. B. 1970, *ApSS*, 7, 3
- Sunyaev, R. A. & Zel'dovich, Y. B. 1972, *CoASP*, 4, 173
- White, D. A., Jones, C., & Forman, W. 1997, *MNRAS*, 292, 419

CLUSTER TEMPLATE

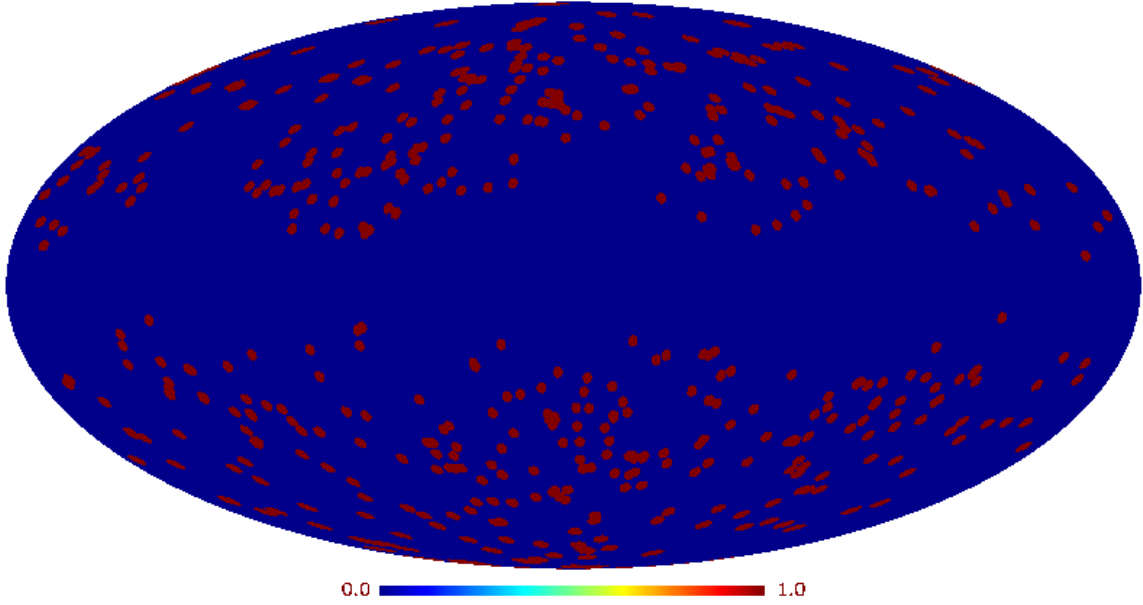


FIG. 1.— Distribution on the sky of the 506 clusters of our sample in Healpix format. Clusters are plotted as discs of radius 1.5° for easier visualization.

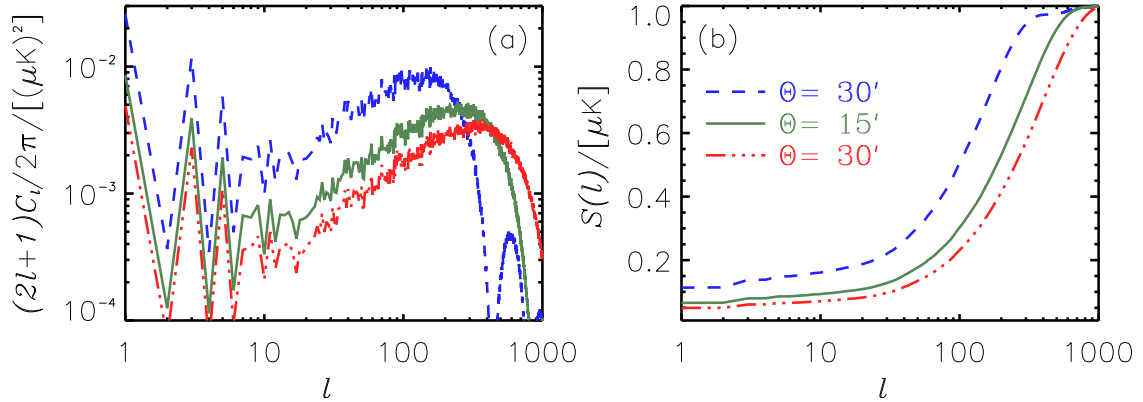


FIG. 2.— (a) Power spectrum of a KSZ dipole generated by 506 identical clusters of different sizes: $30'$ (dashed blue line), $15'$ (solid green) and $10'$ (dot-dashed red), moving in the direction of the CMB dipole with an amplitude of $D = 1\mu\text{K}$. (b) Integrated signal (eq. 3) for the same three angular sizes; lines follow the same convention than in (a).

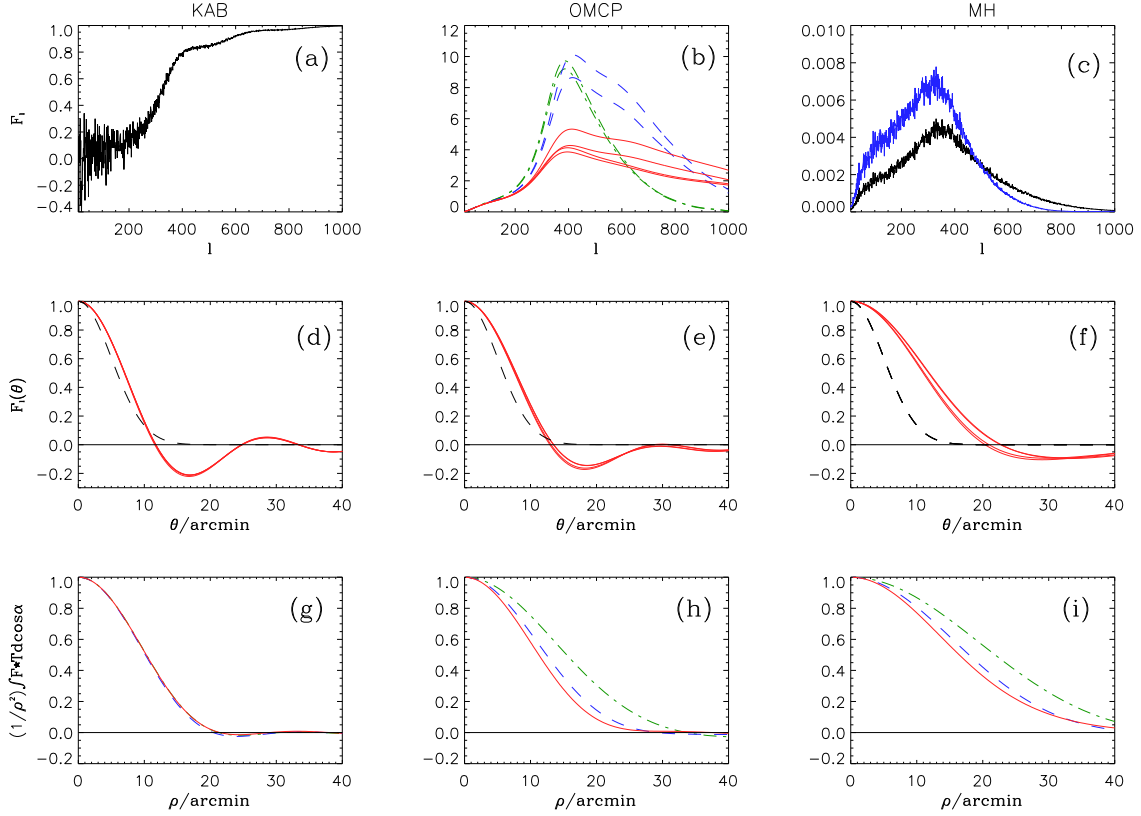


FIG. 3.— Filters in (top to bottom) ℓ space (a-c), real space (d-f), and signal integrated over a disc of angular radius ρ (g-i) for (left to right) the three different filters defined by KAB, OMCP, and MH discussed in Sec. 2. (a) KAB filter for the WMAP W1 DA. (b) OMCP filters for the Q (dot-dashed green line), V (dashed blue line) and W (solid red) channels. (c) MH filters, computed assuming that all clusters have the same angular size of either 10' (black line) or 15' (blue line). (d–f) The respective W-band filters in real space (red, solid line). The dashed line corresponds to a gaussian antenna with the resolution of the W-band. (g–i) Filter averaged over an aperture of size ρ as a function of aperture size. The lines follow the same convention as in (b).

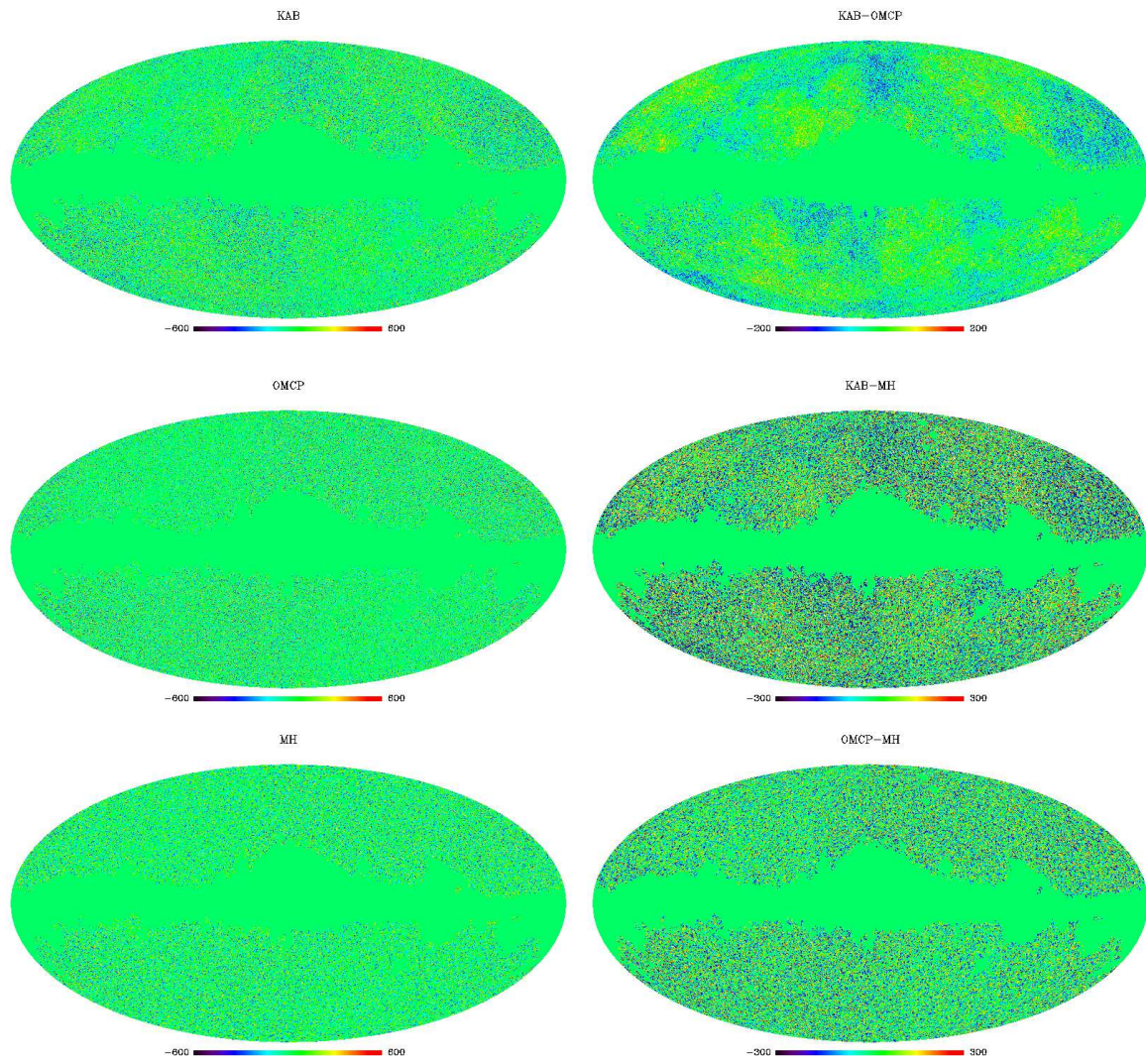


FIG. 4.— Filtered maps in Healpix format. Left column and from top to bottom: W1 DA map filtered using the KAB, OMCP and MH filters. Right column: differences between the various filtered maps.

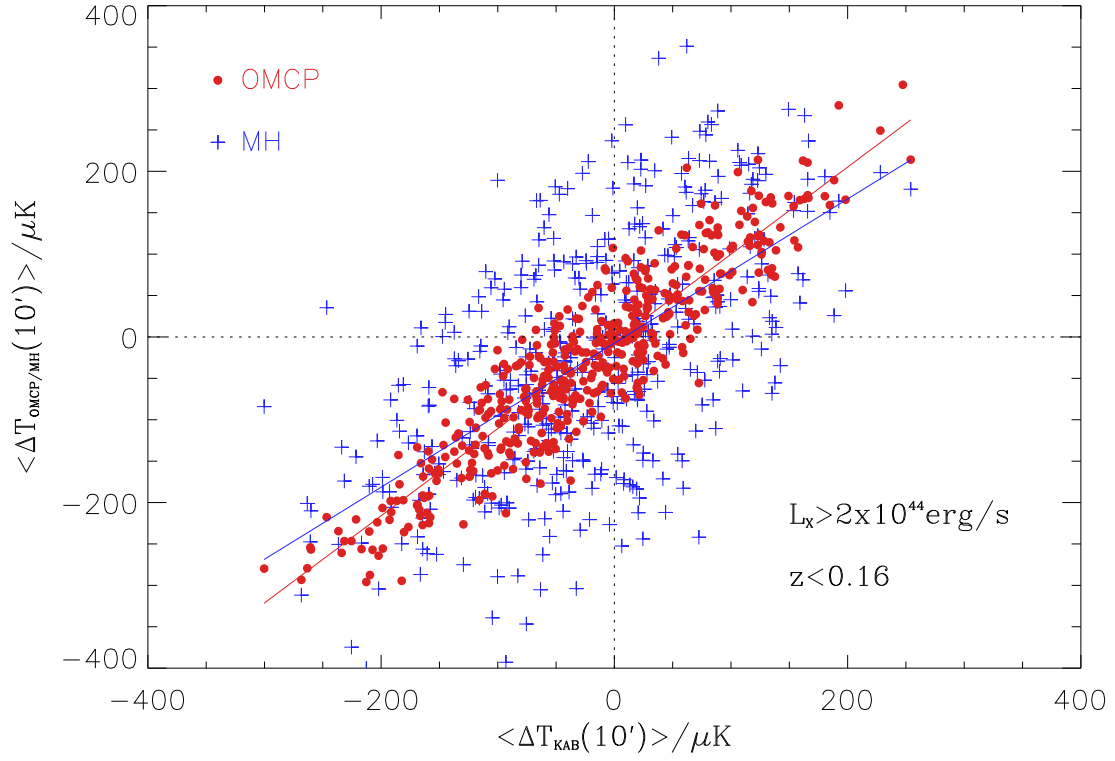


FIG. 5.— Mean temperature anisotropy on a disc of radius 10' at each cluster location for clusters of sample III. Red circles correspond to OMCP vs KAB filter and blue crosses to MH vs KAB. Straight lines were obtained by minimum square regression.

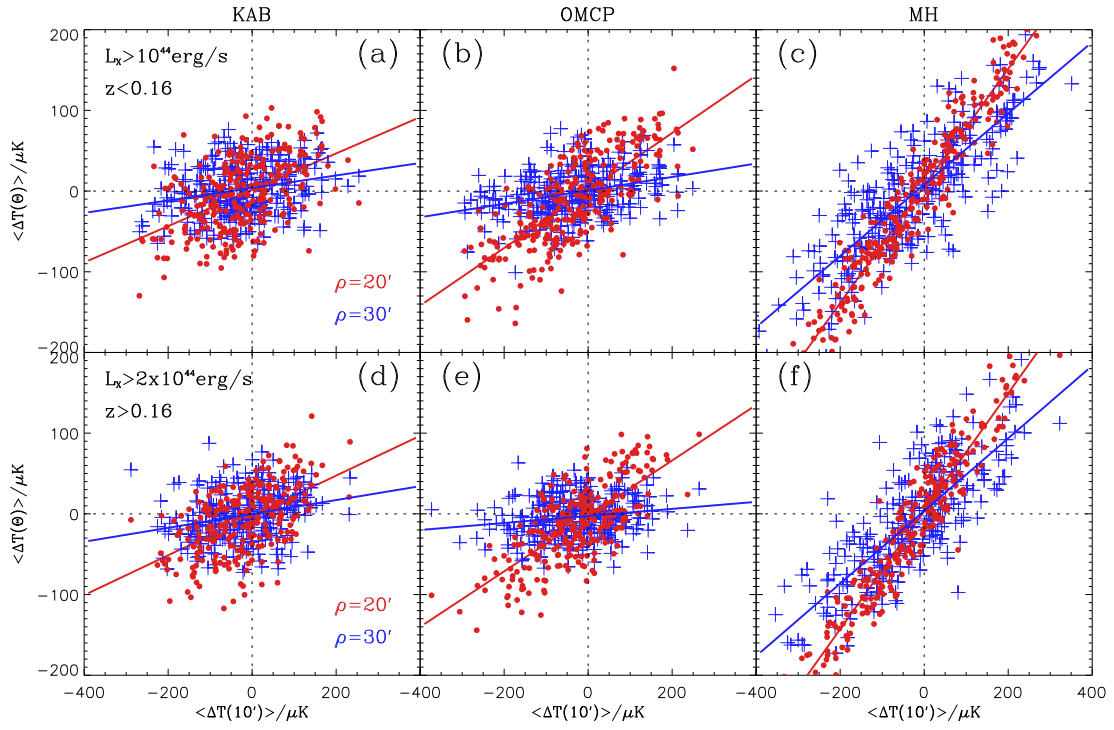


FIG. 6.— Mean temperature anisotropy on the filtered W1 DA, averaged over discs of radius $\rho = 20'$ and $30'$ versus $10'$, for the three filters and for two cluster configurations. Red dots and blue crosses correspond to $20'$ and $30'$, respectively. The solid line is the minimum square regression fit.

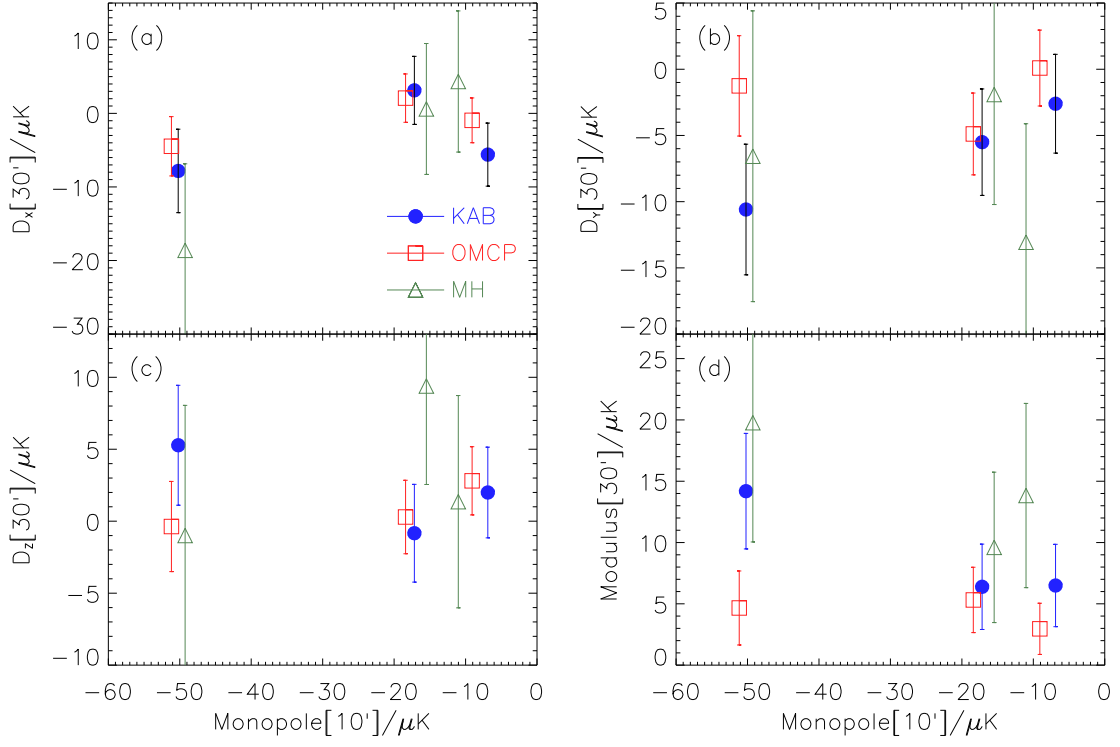


FIG. 7.— X, Y, and Z components of the dipole and modulus of the dipole evaluated within 30' for the KAB (filled circles), OMCP (open squares) and MH (triangles) filters, respectively, versus the monopole at 10' aperture for the three samples given in Table 1. Error bars are obtained from 4,000 simulations of clusters templates randomly placed on the filtered maps.